

Enhancement of Atmospheric Nucleation by Highly Oxygenated Organic Molecules: A Density Functional Theory Study

Feng Zhao,^{†,‡} Ya-Juan Feng,^{*,‡} Yi-Rong Liu,[‡] Shuai Jiang,[‡] Teng Huang,[†] Zi-Hang Wang,[‡] Cai-Xin Xu,[‡] and Wei Huang^{*,†,‡,§}

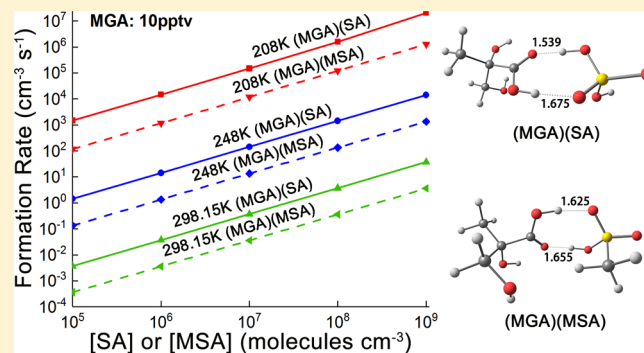
[†]Laboratory of Atmospheric Physico-Chemistry, Anhui Institute of Optics & Fine Mechanics, Chinese Academy of Sciences, Hefei, Anhui 230031, China

[‡]School of Information Science and Technology, University of Science and Technology of China, Hefei, Anhui 230026, China

[§]Center for Excellent in Urban Atmospheric Environment, Institute of Urban Environment, Chinese Academy of Sciences, Xiamen, Fujian 361021, China

Supporting Information

ABSTRACT: New particle formation (NPF) by gas–particle conversion is the main source of atmospheric aerosols. Highly oxygenated organic molecules (HOMs) and sulfuric acid (SA) are important NPF participants. 2-Methylglyceric acid (MGA), a kind of HOMs, is a tracer of isoprene-derived secondary organic aerosols. The nucleation mechanisms of MGA with SA were studied using density functional theory and atmospheric cluster dynamics simulation in this study, along with that of MGA with methanesulfonic acid (MSA) as a comparison. Our theoretical works indicate that the (MGA)(SA) and (MGA)(MSA) clusters are the most stable ones in the (MGA)_i(SA)_j (*i* = 1–2, *j* = 1–2) and (MGA)_i(MSA)_j (*i* = 1–2, *j* = 1–2) clusters, respectively. Both the formation rates of (MGA)(SA) and (MGA)(MSA) clusters are quite large and could have significant contributions to NPF. The results imply that the homomolecular nucleation of MGA is unlikely to occur in the atmosphere, and MGA and SA can effectively contribute to heteromolecular nucleation mainly in the form of heterodimers. MSA exhibits properties similar to SA in its ability to form clusters with MGA but is slightly weaker than SA.



1. INTRODUCTION

Atmospheric aerosols have such a profound impact on the global climate, on regional and local weather patterns, and on human health that they have become a major research area for environmental and atmospheric chemists.^{1–6} New particle formation (NPF) by gas–particle conversion is the main source of atmospheric aerosols and consists of two main processes: nucleation and the subsequent growth of critical nuclei.^{7–9} Thus, studies of the formation process of critical nuclei are crucial for revealing the nucleation mechanism. Although NPF has received widespread attention and has been studied for a considerable period of time, the mechanisms of nucleation and the species involved in it at the molecular cluster level are still unclear.^{9–13}

Sulfuric acid (H₂SO₄, SA) has been widely recognized as a major atmospheric nucleation species.^{8,14,15} However, the binary nucleation of SA and water is not sufficient to account for the nucleation rate measured in the actual atmospheric environment.^{16,17} Therefore, other substances may participate in the formation of critical nuclei. Organic acids are such a candidate^{8,13,18–21} because they can form larger stable heterodimers with SA. Numerous studies have proposed that

the oxidation products of volatile organic compounds (VOCs) participate in NPF,^{11,22–29} among which highly oxygenated organic molecules (HOMs) makes a prominent contribution.^{25–34}

Almost half (40–50%) of the atmospheric fine aerosol mass is contributed by secondary organic aerosols (SOAs), which are produced by the oxidation of VOCs.^{35–37} Isoprene (2-methyl-1,3-butadiene, C₅H₈) is a ubiquitous biological source of VOCs in the troposphere and has a discharge rate of 500–600 Tg year⁻¹.^{38,39} It has been confirmed that photo-oxidation of isoprene causes a large amount of SOA formation.^{40,41} Isoprene-derived SOAs are expected to form 30–50% of total SOAs on the global scale.^{42,43} However, the formation mechanism of isoprene-derived aerosols is still unknown. 2-Methylglyceric acid (C₄H₈O₄, MGA), a further oxidation product of isoprene, is a tracer of isoprene-derived SOAs.^{44–46} MGA has been repeatedly discovered in NPF events in laboratory studies and atmospheric observations,^{44–61} suggest-

Received: April 4, 2019

Revised: May 21, 2019

Published: June 4, 2019

ing that MGA is a potential participant in SOA formation. During survey cruises from the Bohai Sea to the high Arctic in 2003 and from the East China Sea to the Northwest Pacific in 2014, MGA was found to be dominant among SOA tracers.^{55,56} Moreover, MGA makes significant contributions to SOA samples collected in the marine boundary layer from the Arctic to the Antarctic.⁵⁷ Furthermore, MGA is a dihydroxy acid (including two hydroxyl groups and one carboxyl group), so it is highly likely to form hydrogen bonds (HBs) with potential nucleation molecules. At present, little research has been conducted on the nucleation reactions of MGA. Therefore, theoretical calculations were performed in order to investigate its potential nucleation reactions.

Methanesulfonic acid (CH₃SO₃H, MSA) and SA are the two main oxidation products of dimethyl sulfide released from the ocean into the atmosphere.^{62,63} In coastal and marine areas, the concentration of MSA lies in the range 10⁵ to 10⁷ molecules cm⁻³.^{64–67} In field observations, laboratory studies and theoretical studies, MSA has been found to play a major role in NPF events.^{68–77} Okuyama and co-workers systematically studied MSA–water binary nucleation and found that undersaturated MSA vapor can generate aerosols with a concentration of up to 10⁵ molecules cm⁻³ at moderate relative humidity (<60%).^{68,69} Dall’Osto et al. found a decrease in MSA concentration during the NPF events in the oceanic atmosphere, suggesting that MSA may participate in the formation of initial clusters and contribute to their further growth.⁷⁰ Extensive studies by the Finlayson-Pitts group at the University of California, Irvine, have shown that MSA can form clusters with amines and water.^{71–76} In addition, organic acids have been shown to promote the particle formation and further growth of MSA with amines.⁷⁸

Recently, nucleation events involving HOMs and SA have been extensively studied and are considered to be the key components of NPF.^{8,13,18–21,27,79} Some studies suggest that the initial clusters of HOMs contain only one organic molecule^{19,20} and one or two SA molecules.¹⁹ Zhang then proposed the possibility of a large organic acid molecule and two SA molecules forming a stable initial cluster.⁸ Further experiments by Schobesberger et al. demonstrated that HOMs, produced by monoterpene oxidation, form initial clusters with a single SA molecule and then grow into clusters containing one to three SA molecules and one to four HOMs.⁷⁹ However, the nucleation mechanisms of HOMs with SA have not been studied exactly in detail, especially the oxidation products of isoprene, MGA. Thus, this paper will analyze the microscopic mechanism of nucleation between MGA and SA, and the clusters containing one MGA molecule and one or two SA molecules will be carefully analyzed. The nucleation mechanism between MGA and MSA will also be studied for comparison. In addition, because Zhang et al.⁵⁰ and Nestorowicz et al.⁵¹ have demonstrated that the nucleated yield of isoprene aerosol is higher at low humidity, the contribution of water could be ignored.

2. METHODS

2.1. Structural Calculations. The initial structures of (MGA)_i(SA)_j (*i* = 1–2, *j* = 1–2) and (MGA)_i(MSA)_j (*i* = 1–2, *j* = 1–2) clusters were obtained by using the basin-hopping algorithm coupled with the semi-empirical PM7 method implemented in MOPAC2016.^{80–83} Then, the low-energy isomers were further optimized at the M06-2X/6-311++G(3df,3pd) theory level. The M06-2X method performs

well at simulating atmospheric clusters containing common organic acids and produces similar results compared with experimental results and those of DLPNO-CCSD(T)/aug-cc-pVTZ theory level.^{84–89} To ensure that there are no imaginary frequencies in the clusters, frequency calculations were also performed. The optimizations were implemented using the Gaussian 09 programs with default convergence criteria.⁹⁰ The single-point energy was calculated at the DF-MP2-F12/VDZ-F12 theory level,⁹¹ implemented with the MOLPRO 2010.1.^{92,93} Thermodynamic parameters were evaluated from the thermodynamic corrections calculated by M06-2X/6-311++G(3df,3pd) combined with the single-point energies obtained from DFT-MP2-F12/VDZ-F12. In order to evaluate the performance of DF-MP2-F12/VDZ-F12 theory level, we calculated the single-point energy of reactions (MGA) + SA ↔ (MGA)(SA) and (MGA)(SA) + SA ↔ (MGA)(SA)₂ at the DLPNO-CCSD(T)/aug-cc-pVTZ theory level. The binding energies (ΔE) and the formation enthalpies (ΔH) calculated at DF-MP2-F12/VDZ-F12//M06-2X/6-311++G(3df,3pd) and DLPNO-CCSD(T)/aug-cc-pVTZ//M06-2X/6-311++G(3df,3pd) theory levels are listed in Table S1 in the [Supporting Information](#). Both the differences of ΔE and ΔH values obtained by the two calculated levels are approximately 0.7 kcal mol⁻¹, suggesting that the DF-MP2-F12/VDZ-F12//M06-2X/6-311++G(3df,3pd) theory level has good performance consistent with the DLPNO-CCSD(T)/aug-cc-pVTZ//M06-2X/6-311++G(3df,3pd) theory level in calculating binding energies and formation enthalpies.

2.2. Atmospheric Cluster Dynamics Simulation.

Thermodynamic data calculated at the DF-MP2-F12/VDZ-F12//M06-2X/6-311++G(3df,3pd) level were studied by cluster dynamics simulations based on the Atmospheric Cluster Dynamics Code (ACDC) kinetic model.⁹⁴ The simulations involve collisions of all possible clusters of the studied system and perform well for systems containing organic acids.^{95–98} The time evolution of molecular cluster distributions can be studied by explicitly solving the birth–death equation given by eq 1

$$\frac{dc_i}{dt} = \frac{1}{2} \sum_{j < i} \beta_{j,(i-j)} c_j c_{(i-j)} + \sum_j \gamma_{(i+j) \rightarrow i} c_{(i+j)} - \sum_j \beta_{i,j} c_i c_j - \frac{1}{2} \sum_{j < i} \gamma_{i \rightarrow j} c_i + Q_i - S_i \quad (1)$$

where *i* and *j* are the clusters in the given system, β_{ij} is the collision coefficient between the two clusters *i* and *j*, $\gamma_{i \rightarrow j}$ is the evaporation coefficient of cluster *i* split into *j* and another smaller cluster, *c_i* and *c_j* are the concentrations of clusters *i* and *j*, *Q_i* is an additional source term of cluster *i*, and *S_i* is a possible loss term of cluster *i*. The collision coefficients β_{ij} obtained from kinetic gas theory are calculated from eq 2

$$\beta_{i,j} = \left(\frac{3}{4\pi} \right)^{1/6} \left(\frac{6k_b T}{m_i} + \frac{6k_b T}{m_j} \right)^{1/2} (V_i^{1/3} + V_j^{1/3})^2 \quad (2)$$

where *T* is the temperature, *k_b* is the Boltzmann constant, *m_i* is the mass of cluster *i*, and *V_i* is the volume of cluster *i*. The calculations of the evaporation coefficients $\gamma_{(i+j) \rightarrow j}$ are given by eq 3

$$\gamma_{(i+j) \rightarrow i,j} = \beta_{i,j} \frac{c_i^e c_j^e}{c_{i+j}^e} = \beta_{i,j} c_{\text{ref}} \exp\left(\frac{\Delta G_{i+j} - \Delta G_i - \Delta G_j}{k_b T}\right) \quad (3)$$

where $\beta_{i,j}$ is the collision coefficient between clusters i and j , ΔG_i is the Gibbs free energy of formation of cluster i , c_i^e is the equilibrium concentration of cluster i , and c_{ref} represents the monomer concentration of the reference vapor at which the free energies have been calculated.

The formation rate in our study is defined as “the flux of clusters outside the system.”⁹⁴ We set different boundary sizes to study the contribution of MGA–SA and MGA–MSA clusters of various sizes to NPF. The formation rates of all clusters in the system were obtained by ACDC. The systems we studied were acid–acid systems, which differed from the acid–base system of McGrath et al.⁹⁴ In the acid–base system simulation, the homonuclear nucleation of the base should be ignored, so the cluster should contain at least one acid molecule. However, for the acid–acid system simulation, the homonuclear nucleation of both kinds of acids should not be ignored [e.g., (SA)₂ and (MGA)₂ clusters], so the number of acid molecules in the clusters should be increased from 0. Therefore, the formula for calculating the formation rates⁹⁴ can be rewritten as eq 4

$$J = \sum_{i=0}^m \sum_{j=0}^m \sum_{k=0}^n \sum_{l=0}^n \beta_{ik,jl} c_{ik} c_{jl}, \quad (i+k > 0, j+l > 0) \quad (4)$$

where m and n are the boundaries of the system, c_{ik} is the concentration of cluster ik , i and j stand for the number of SA–MSA molecules in clusters ik and jl , respectively, and k and l stand for the number of MGA molecules in clusters ik and jl , respectively. The temperature dependence of the formation rates was studied by inputting entropy (ΔS) and enthalpy (ΔH) instead of Gibbs free energy ($\Delta G = \Delta H - T\Delta S$).

3. RESULTS AND DISCUSSION

3.1. Structures. The geometries of the global minima for monomers and (MGA)(SA)_{*m*} ($m = 1-2$) and (MGA)(MSA)_{*n*} ($n = 1-2$) clusters calculated at the M06-2X/6-311++G-(3df,3pd) theory level are shown in Figure 1. The structures of the clusters containing two MGA molecules are shown in Figure S1 in the Supporting Information. The Cartesian coordinates of all the structures are listed in Table S2 in the Supporting Information.

The MGA monomer has one carboxyl group and two hydroxyl groups. In order to distinguish the two hydroxyl groups in MGA, the hydroxyl group linking a methylene group is called the α -hydroxyl group and the hydroxyl group linking a single carbon atom is called the β -hydroxyl group. For (MGA)(SA), two O–H...O HBs with lengths of 1.539 and 1.675 Å are formed between the carboxyl group of MGA and SA. For (MGA)(SA)₂, one MGA molecule and two SA molecules are contacted by forming four HBs. The lengths of the four HBs are 1.524, 1.698, 1.636, and 1.645 Å. For (MGA)(MSA), two HBs with lengths of 1.625 and 1.655 Å are formed between the carboxyl group of MGA and MSA. For (MGA)(MSA)₂, one MGA molecule and two MSA molecules are contacted by three strong HBs. The lengths of the three HBs (HB₁, HB₂, and HB₃ in the Figure 1) are 1.532, 1.598, and 1.640 Å, respectively. In the (MGA)(MSA)₂ cluster, the free α -hydroxyl group of MGA participates in the formation of

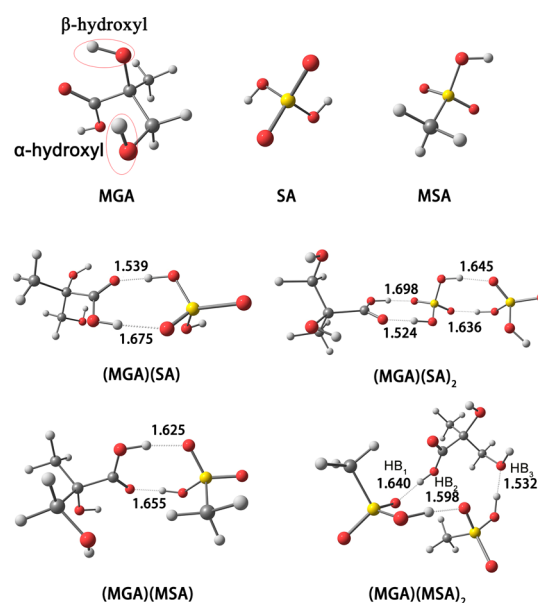


Figure 1. Geometries of the global minima for monomers and (MGA)(SA)_{*m*} ($m = 1-2$) and (MSA)(SA)_{*n*} ($n = 1-2$) clusters optimized at the M06-2X/6-311++G(3df,3pd) theory level.

HBs. As shown in Figure 1, for the length of HBs in the (MGA)(MSA)₂ cluster, HB₁ < HB₂ < HB₃, indicating that the closer the HB is to the α -hydroxyl group of MGA, the shorter the HB length is. Compared with the (MGA)(MSA) cluster, the addition of an MSA molecule to the (MGA)(MSA) cluster causes one of the HBs to break and recombine, resulting in further HBs forming and shorter HB lengths. In all the structures, the carboxyl group of MGA participates in the formation of HBs, and the hydroxyl group of MGA participates in the formation of HBs only in the (MGA)(MSA)₂ structure, indicating that the carboxyl group in MGA has a greater ability to form HBs than the hydroxyl group.

3.2. Intermolecular Interactions. Topological analysis of electron densities can demonstrate the presence of HBs in the cluster. Bader’s theory of “atoms in molecules” (AIM) is considered to be one of the most effective tools for exploring interactions between molecules, such as HBs.^{99–103} In this paper, therefore, the AIM theory is applied in order to evaluate the properties of intermolecular hydrogen bonding interactions in the (MGA)(SA)_{*m*} ($m = 1-2$) and (MGA)(MSA)_{*n*} ($n = 1-2$) clusters. In order to analyze the topological characteristics of the bond critical points (BCPs), the electron density (ρ), its Laplacian electron density ($\nabla^2\rho$), the electronic energy density (H), the electronic kinetic energy density (G), and the electronic potential energy density (V) calculated by the Multiwfn program¹⁰⁴ are listed in Table 1.

The strength of a HB is related to ρ , and generally, the larger the ρ value, the stronger the HB. A quantitative criterion has been proposed to characterize the strength of HBs: ρ , in the range of 0.002–0.035 a.u.¹⁰⁵ As listed in Table 1, the ρ values of the HBs in all of the (MGA)(SA)_{*m*} ($m = 1-2$) and (MGA)(MSA)_{*n*} ($n = 1-2$) clusters were in the range 0.042–0.070 a.u., and these values exceeded the upper limit of the standard electron density range. High values of ρ indicate that the hydrogen bonding interactions in the (MGA)(SA)_{*m*} ($m = 1-2$) and (MGA)(MSA)_{*n*} ($n = 1-2$) clusters are quite strong. The values of $\nabla^2\rho$ and H are related to the nature of the interaction. A negative value of $\nabla^2\rho$ indicates the presence of a

Table 1. Topological Parameters of the BCPs in (MGA)(SA)_m (*m* = 1–2) and (MGA)(MSA)_n (*n* = 1–2) Clusters at the M062X/6-311++G(3df,3pd) Theory Level^a

isomers	BCPs	$\rho/\text{a.u.}$	$\nabla^2\rho/\text{a.u.}$	$G/\text{a.u.}$	$V/\text{a.u.}$	$H/\text{a.u.}$	$-G/V$
(MGA)(SA)	CH ₃ COH(CH ₂ OH)COHO...H-OSO ₃ H	0.067	0.100	0.050	-0.076	-0.025	0.67
	CH ₃ COH(CH ₂ OH)COO-H...OSO(OH) ₂	0.045	0.119	0.038	-0.047	-0.009	0.82
(MGA)(SA) ₂	CH ₃ COH(CH ₂ OH)COHO...H-OS ¹ O ₃ H	0.070	0.099	0.052	-0.079	-0.027	0.66
	HOS ¹ O ₂ O-H...O=S ² O ₂ OH	0.049	0.119	0.041	-0.053	-0.011	0.78
	HOS ¹ O ₂ HO...H-OS ² O ₂ OH	0.047	0.121	0.041	-0.051	-0.010	0.80
	CH ₃ COH(CH ₂ OH)COO-H...OS ¹ O(OH) ₂	0.042	0.118	0.036	-0.043	-0.007	0.84
(MGA)(MSA)	CH ₃ COH(CH ₂ OH)COO-H...OSO ₂ HCH ₃	0.059	0.115	0.043	-0.058	-0.014	0.75
	CH ₃ COH(CH ₂ OH)COHO...H-OSO ₂ CH ₃	0.049	0.115	0.040	-0.052	-0.012	0.78
(MGA)(MSA) ₂	CH ₃ COH(COOH)CH ₂ -HO...H-OS ² O ₂ CH ₃	0.069	0.104	0.052	-0.078	-0.026	0.67
	CH ₃ S ¹ O ₂ O-H...OS ² O ₂ HCH ₃	0.056	0.110	0.045	-0.062	-0.017	0.72
	CH ₃ COH(CH ₂ OH)COO-H...OS ¹ O ₂ HCH ₃	0.049	0.119	0.041	-0.053	-0.012	0.78

^aThe superscripts are used to label the different sulfur atoms in (MGA)(SA)₂ and (MGA)(MSA)₂, wherein the sulfur atom in the SA or MSA molecule attached to the carboxyl group of MGA is denoted as S¹ and the other sulfur atom is denoted as S².

shared interaction, such as a covalent bond; a positive value of $\nabla^2\rho$ indicates a closed-shell system interaction, that is, an ionic interaction, a van der Waals force, or a HB. In the case where the $\nabla^2\rho$ value is positive, a negative H value demonstrates that the interaction is partially covalent, and a positive H value demonstrates that the strength of the HB interaction is weak. As listed in Table 1, all the BCPs have positive $\nabla^2\rho$ values and negative H values, indicating that all the interactions are partially covalent. In addition, the value of $-G/V$ indicates a region corresponding to a covalent or noncovalent interaction (NCI). If the $-G/V$ value is greater than 1, the interaction is noncovalent; if the $-G/V$ value is between 0.5 and 1, the interaction is partially covalent; if the $-G/V$ value is less than 0.5, the interaction is covalent. As listed in Table 1, all the BCPs have a $-G/V$ value between 0.5 and 1, indicating that all interactions are partially covalent in nature. Gilli and co-workers reported that HBs are mainly electrostatic and become covalent as the bond strength increases.^{106–109} As a consequence of the partially covalent nature of the HBs in the (MGA)(SA)_m (*m* = 1–2) and (MGA)(MSA)_n (*n* = 1–2) clusters, all of the HBs are quite strong.

Yang and co-workers proposed the NCIs index based on the relationship between the electron density and the reduced density gradient (RDG).^{110,111} RDG(*s*) was calculated from eq 5 in order to demonstrate the deviation from a homogeneous electron distribution^{112,113}

$$s = \frac{1}{2(3\pi)^{1/3}} \frac{|\nabla\rho|}{\rho^{4/3}} \quad (5)$$

where ρ is the electron density based on M06-2X/6-311++G(3df,3pd), ∇ is the gradient operator, and $|\nabla\rho|$ is the electronic density gradient mode. Here, the NCI analysis method can be seen as an extension of AIM: it not only confirms NCIs and covalent interactions in real space but also visualizes the properties around BCPs.

Figure 2 shows the plots of RDG versus $\text{sign}(\lambda_2)$ multiplied by ρ and the visualized gradient isosurfaces, obtained from Multiwfn¹⁰⁴ and VMD,¹¹⁴ respectively, for the global minima of (MGA)(SA)_m (*m* = 1–2) and (MGA)(MSA)_n (*n* = 1–2), where λ_2 is the second Hessian eigenvalue. When the $\text{sign}(\lambda_2)\rho$ values corresponding to the peak are close to zero, the interaction is weak, such as for van der Waals forces, as shown in the green area. The negative $\text{sign}(\lambda_2)\rho$ value corresponds to the HB, and when the $\text{sign}(\lambda_2)\rho$ value is more negative, the strength of HB is stronger; the positive $\text{sign}(\lambda_2)\rho$ value

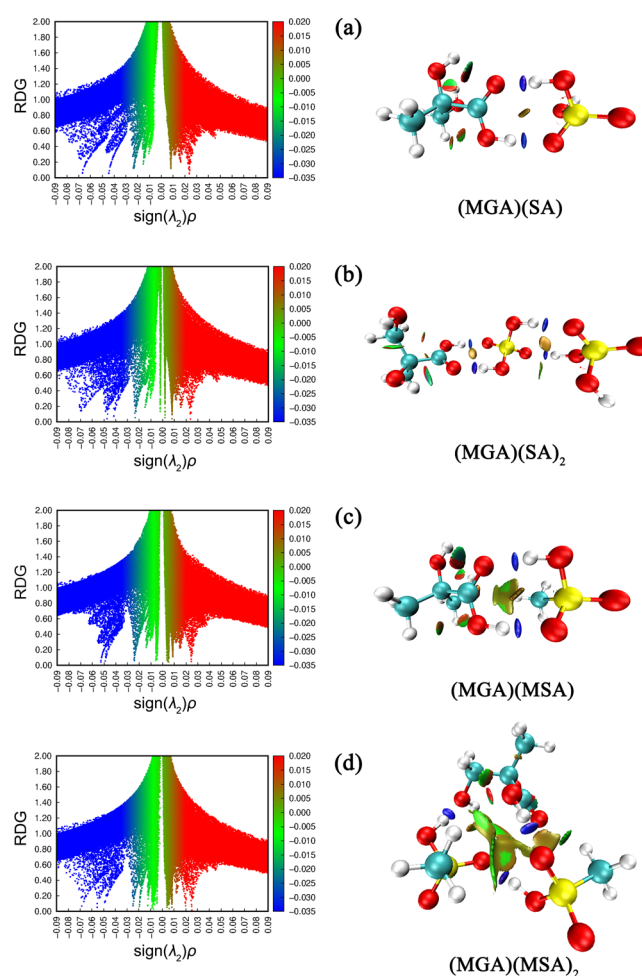


Figure 2. Plots of RDG vs $\text{sign}(\lambda_2)$ multiplied by ρ and the visualized gradient isosurfaces for the global minima of (a) (MGA)(SA), (b) (MGA)(SA)₂, (c) (MGA)(MSA), and (d) (MGA)(MSA)₂.

corresponds to the steric hindrance, and when the $\text{sign}(\lambda_2)\rho$ value is more positive, the strength of steric hindrance is stronger. It can be seen from the plots of RDG(*s*) versus $\text{sign}(\lambda_2)\rho$ that all clusters have HBs (blue area), and the HBs are stronger than the steric hindrance (red area), revealing that weak interactions are dominant in these clusters. The gradient isosurfaces on the right-hand of Figure 2 show the HBs corresponding to the plots of RDG(*s*) versus $\text{sign}(\lambda_2)\rho$ on the

left-hand of Figure 2. All blue gradient isosurfaces correspond exactly to the HBs in Figure 1. The peak corresponding to the sign(λ_2) ρ value of 0.48 a.u. in Figure 2b is obtained from two peaks coinciding with each other and represents two HBs. The results shown that intermolecular interactions between MGA and SA or MSA are quite strong HBs, and the (MGA)(SA)_{*i*} (*i* = 1–2) clusters have comparable HBs strengths and properties with the corresponding (MGA)(MSA)_{*i*} (*i* = 1–2) clusters. The results of the NCI index analysis are consistent with the AIM results.

3.3. Thermochemical Analysis. Analysis of thermodynamic properties can characterize the possibility of cluster formation in the atmosphere. Thus, we have studied the relative zero-point correction energies ΔE (0 K), enthalpies ΔH (298.15 K), and Gibbs free energies ΔG (298.15 K) of the global minima of (MGA)(SA)_{*m*} (*m* = 1–2) and (MGA)-(MSA)_{*n*} (*n* = 1–2) clusters in detail. Zero-point correction energies and other thermodynamic parameters were calculated at the DF-MP2-F12/VDZ-F12//M06-2X/6-311++G(3df,3pd) level. The calculation of the thermodynamic parameter changes in the reaction follows the reaction processes. For example, ΔG (298.15 K) of the reaction (MGA)(SA)_{*m-1*} + SA \leftrightarrow (MGA)(SA)_{*m*} (*m* = 1–2) was calculated using eq 6.

$$\Delta G_m = G_{(\text{MGA})(\text{SA})_m} - G_{(\text{MGA})(\text{SA})_{m-1}} - G_{(\text{SA})} \quad (6)$$

Table 2 lists the thermodynamic parameter changes in the formation of (MGA)(SA)_{*m*} (*m* = 1–2) and (MGA)(MSA)_{*n*} (*n* = 1–2) clusters.

Table 2. Thermodynamic Parameter Changes for the Formation of (MGA)(SA)_{*m*} (*m* = 1–2) and (MGA)(MSA)_{*n*} (*n* = 1–2) Clusters Calculated at the DF-MP2-F12/VDZ-F12//M06-2X/6-311++G(3df,3pd) Theory Level^a

reactions	ΔE (0 K)	ΔH (298.15 K)	ΔG (298.15 K)
MGA + SA \leftrightarrow (MGA)(SA)	-16.64	-17.16	-5.55
(MGA)(SA) + SA \leftrightarrow (MGA)(SA) ₂	-16.61	-15.91	-7.83
MGA + MSA \leftrightarrow (MGA)(MSA)	-16.79	-16.95	-4.64
(MGA)(MSA) + MSA \leftrightarrow (MGA)(MSA) ₂	-15.55	-15.56	-3.77

^aThe units are kcal mol⁻¹.

= 1–2). The ΔG values of (MGA)(SA) and (MGA)(SA)₂ are -5.55 and -7.83 kcal mol⁻¹, respectively, and those of (MGA)(MSA) and (MGA)(MSA)₂ are -4.64 and -3.77 kcal mol⁻¹, respectively. The ΔG values for all the reaction paths are negative, meaning that all reactions can take place spontaneously. The binding energies of (MGA)(SA) and (MGA)(SA)₂ are -16.64 and -16.61 kcal mol⁻¹, respectively, and those of (MGA)(MSA) and (MGA)(MSA)₂ are -16.79 and -15.55 kcal mol⁻¹, respectively. Compared with (MGA)(SA), (MGA)(MSA) has comparable binding energy (-16.64 and -16.79 kcal mol⁻¹) and formation enthalpy (-17.16 and -16.95 kcal mol⁻¹). Compared with (MGA)(SA)₂, (MGA)(MSA)₂ also has comparable binding energy change (-16.61 and -15.55 kcal mol⁻¹) and formation enthalpy (-15.91 and -15.56 kcal mol⁻¹). The combination of MGA and SA or MSA is supported by favorable thermodynamic properties. The (MGA)(SA)_{*i*} (*i* = 1–2) clusters have comparable stability to corresponding (MGA)(MSA)_{*i*} (*i* = 1–2) clusters, which is consistent with the result of topological analyses.

3.4. Temperature Dependence of Conformational Populations. Clusters of a certain size in the atmosphere have

different isomers, and its contribution to NPF is assessed by statistical average of the contributions of all isomers.^{115–118}

The conformational populations and thermodynamic properties of the isomers are affected by temperature, so it is necessary to study the temperature dependence of conformational populations.^{115–118} The conformational populations of (MGA)(SA)_{*m*} (*m* = 1–2) and (MGA)(MSA)_{*n*} (*n* = 1–2) clusters associated with temperature are shown in Figure 3.

For (MGA)(SA)_{*m*} (*m* = 1–2), the conformational populations of the global minima of (MGA)(SA) and (MGA)(SA)₂ consistently account for nearly 100% in the range 50–350 K, and other isomers are not competitive. Similar to (MGA)(SA)_{*m*} (*m* = 1–2), the global minima of (MGA)(MSA)_{*n*} (*n* = 1–2) are also dominant. For (MGA)(MSA) (Figure 3c), the population of the global minimum 1.1-a decreases slightly with increasing temperature from 250 to 350 K, but still accounts for 93.81% at 350 K. The population of isomer 1.1-b increases slightly, accounting for 6.16% at 350 K. All the (MGA)(SA)_{*m*} (*m* = 1–2) and (MGA)(MSA)_{*n*} (*n* = 1–2) clusters show weak temperature dependence for conformational populations, and the global minima of these clusters are continuously dominant, indicating that the global minima are the primary configurations leading to NPF. Thus, it is reasonable to study the global minima of these clusters in this paper.

3.5. Atmospheric Cluster Dynamics Simulation.

3.5.1. Evaporation Rates. Previous studies have shown that the cluster evaporation rate is an important parameter for understanding the early stages of NPF.^{94,119} Figure 4 shows the total evaporation rates of (MGA)(SA)_{*m*} (*m* = 1–2) and (MGA)(MSA)_{*n*} (*n* = 1–2) clusters as a function of temperature. For (MGA)(SA)_{*m*} (*m* = 1–2) clusters, when the temperature varies from 200 to 320 K, the evaporation rates of (MGA)(SA) and (MGA)(SA)₂ range from 10⁻¹ to 10⁶ s⁻¹ and from 10⁰ to 10⁶ s⁻¹, respectively. The evaporation rate of (MGA)(SA) is consistently lower than that of (MGA)(SA)₂ in the range 200–320 K. For (MGA)(MSA)_{*n*} (*n* = 1–2) clusters, when the temperature varies from 200 to 320 K, the evaporation rates of (MGA)(MSA) and (MGA)(MSA)₂ vary from 10⁰ to 10⁷ s⁻¹ and from 10⁴ to 10⁹ s⁻¹, respectively. The evaporation rate of (MGA)(MSA)₂ is about 2–4 orders of magnitude higher than that of (MGA)(MSA). In addition, for (MGA)_{*i*}(SA)_{*j*} (*i* = 1–2, *j* = 1–2) and (MGA)_{*i*}(MSA)_{*j*} (*i* = 1–2, *j* = 1–2), the evaporation rates of all clusters at 298.15 K were also investigated and are listed in Table S3 in the Supporting Information. For MGA–SA, the evaporation rates of (MGA)(SA), (MGA)(SA)₂, (MGA)₂(SA), and (MGA)₂(SA)₂ at 298.15 K are 2.90 × 10⁵, 5.01 × 10⁵, 7.40 × 10⁵, and 8.21 × 10¹⁴ s⁻¹, respectively. For MGA–MSA, the evaporation rates of (MGA)(MSA), (MGA)(MSA)₂, (MGA)₂(MSA), and (MGA)₂(MSA)₂ at 298.15 K are 4.00 × 10⁶, 1.50 × 10⁹, 6.26 × 10⁷, and 5.67 × 10¹⁴ s⁻¹, respectively. Thus, for (MGA)_{*i*}(SA)_{*j*} (*i* = 1–2, *j* = 1–2) and (MGA)_{*i*}(MSA)_{*j*} (*i* = 1–2, *j* = 1–2) clusters, the heterodimer has the lowest evaporation rate, indicating that the heterodimer is more stable than the clusters of other sizes. Comparing (MGA)_{*i*}(SA)_{*j*} (*i* = 1–2, *j* = 1–2) with the corresponding (MGA)_{*i*}(MSA)_{*j*} (*i* = 1–2, *j* = 1–2), the clusters of MGA–SA are more stable than those of MGA–MSA, except for the comparison of (MGA)₂(SA)₂ and (MGA)₂(MSA)₂.

Furthermore, regarding whether clusters can exist stably with a certain concentration, two aspects should be mainly

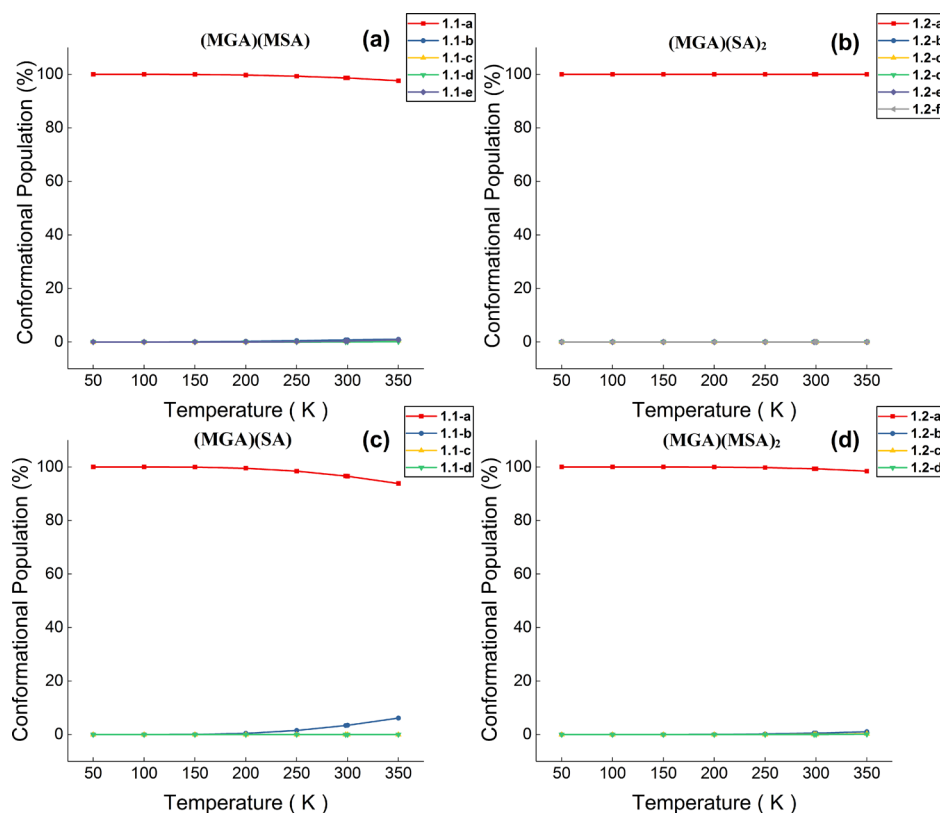


Figure 3. Conformational population changes for the low-energy isomers of $(\text{MGA})(\text{SA})_m$ ($m = 1-2$) and $(\text{MGA})(\text{MSA})_n$ ($n = 1-2$) as a function of temperature from 50 to 350 K.

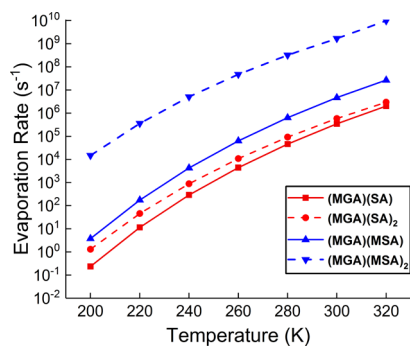


Figure 4. Total evaporation rates of $(\text{MGA})(\text{SA})_m$ ($m = 1-2$) and $(\text{MGA})(\text{MSA})_n$ ($n = 1-2$) vs temperature.

considered: formation by collision of small clusters or monomers and evaporation of the clusters.^{94,120} Assuming equilibrium and detailed balance, the formation and evaporation of clusters are equal (i.e., $F = 0$ in eq 7)^{119,121}

$$F_{(ij,kl)} = \beta_{ij,kl} c_i c_j c_{kl} - \gamma_{ij,kl} c_{ij,kl} \quad (7)$$

where F is the growth flux, c_i is the concentration of the cluster i , β_{ij} is the collision coefficient between clusters i and j , and γ is the evaporation rate. Therefore, when the formation is greater than evaporation, the clusters could be generated with a certain concentration (i.e., $F > 0$ in eq 7).

At 278.15 K, we set the MGA concentration as 10 pptv (2.64×10^{14} molecules m^{-3}) and the concentration of SA or MSA as 10^7 molecules cm^{-3} (10^{13} molecules m^{-3}). For the $(\text{MGA})(\text{SA})$ cluster, the collision coefficient between MGA and SA monomers is 3.75×10^{-16} $\text{m}^3 \text{s}^{-1}$, the total evaporation

rate is $4.49 \times 10^4 \text{ s}^{-1}$, and the final stable concentration obtained by clusters dynamics simulation is 2.20×10^7 molecules m^{-3} . Then, the F value of $(\text{MGA})(\text{SA})$ cluster obtained by eq 7 is $2.20 \times 10^9 \text{ m}^{-3} \text{ s}^{-1}$. For the $(\text{MGA})(\text{MSA})$ cluster, the collision coefficient between MGA and MSA monomers is 4.00×10^{-16} $\text{m}^3 \text{ s}^{-1}$, the total evaporation rate is $5.20 \times 10^5 \text{ s}^{-1}$, and the final stable concentration obtained by clusters dynamics simulation is 2.03×10^6 molecules m^{-3} . Then, the F value of $(\text{MGA})(\text{MSA})$ cluster obtained by eq 7 is $4.00 \times 10^8 \text{ m}^{-3} \text{ s}^{-1}$. Both the F values of $(\text{MGA})(\text{SA})$ and $(\text{MGA})(\text{MSA})$ clusters are positive, indicating that the $(\text{MGA})(\text{SA})$ and $(\text{MGA})(\text{MSA})$ clusters should be stable in MGA–SA and MGA–MSA systems, respectively. In addition, the temperature dependence of the evaporation rates of the $(\text{MGA})(\text{SA})$ and $(\text{MGA})(\text{MSA})$ clusters is consistent with that of the SA dimer (cluster containing two SA molecules), and the stable existence of the SA dimer has been observed in the experiment.^{122,123}

On the basis that the cluster exists stably with a certain concentration, we analyze the flux of the cluster to a large-sized cluster by formation rates in the next section.

3.5.2. Formation Rates. In this study, the formation rates of the clusters in $(\text{MGA})_i(\text{SA})_j$ ($i = 1-2, j = 1-2$) and $(\text{MGA})_i(\text{MSA})_j$ ($i = 1-2, j = 1-2$) systems were analyzed by ACDC. The thermodynamic data calculated at the DF-MP2-F12/VDZ-F12//M06-2X/6-311++G(3df,3pd) level are listed in Table S4 in the Supporting Information. First, the MGA concentration was set at 10 pptv and the concentration of SA or MSA was set in the range 10^5 to 10^9 molecules cm^{-3} . The formation rates of $(\text{MGA})(\text{SA})$, $(\text{MGA})(\text{SA})_2$, $(\text{MGA})(\text{MSA})$, and $(\text{MGA})(\text{MSA})_2$ clusters versus the concentration of SA or MSA at 298.15 K are shown in Figure 5a. For MGA–

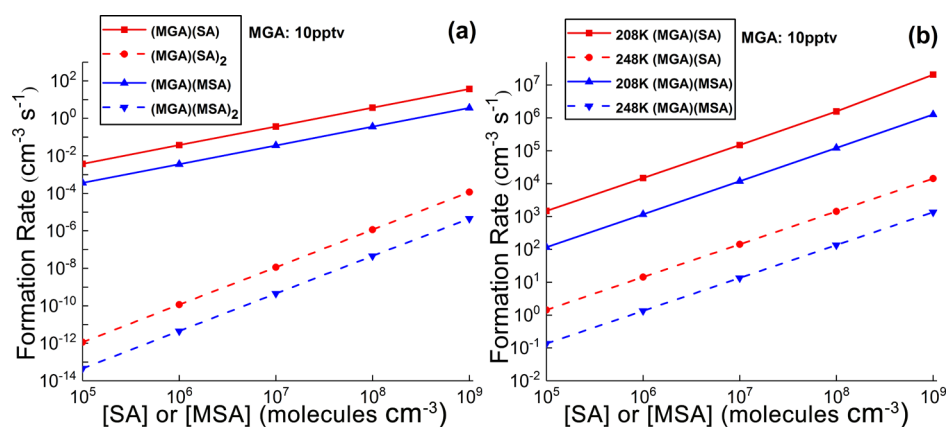


Figure 5. Formation rates of (MGA)(SA), (MGA)(SA)₂, (MGA)(MSA), and (MGA)(MSA)₂ clusters vs the concentration of SA or MSA at (a) 298.15 K, and the formation rates of the (MGA)(SA) and (MGA)(MSA) clusters vs the concentration of SA or MSA at (b) 208 and 248 K.

SA, the formation rates of (MGA)(SA) and (MGA)(SA)₂ vary from 10^{-3} to 10 $\text{cm}^{-3} \text{s}^{-1}$ and from 10^{-12} to 10^{-4} $\text{cm}^{-3} \text{s}^{-1}$, respectively, with the SA concentration varying from 10^5 to 10^9 molecules cm^{-3} . For MGA–MSA, the formation rates of (MGA)(MSA) and (MGA)(MSA)₂ range from 10^{-4} to 10^0 $\text{cm}^{-3} \text{s}^{-1}$ and from 10^{-14} to 10^{-6} $\text{cm}^{-3} \text{s}^{-1}$, respectively, with the MSA concentration ranging from 10^5 to 10^9 molecules cm^{-3} . Both the formation rates of (MGA)(SA) and (MGA)(MSA) clusters are quite large, implying that the (MGA)(SA) and (MGA)(MSA) clusters could play an important role in NPF events, and the formation rates of (MGA)(SA)₂ and (MGA)(MSA)₂ clusters are relatively small.

The temperature dependence of the formation rates of (MGA)(SA) and (MGA)(MSA) were then studied, and the results are shown in Figure 5b. As the temperature decreases, the formation rates of (MGA)(SA) and (MGA)(MSA) increase. At 248 K, when the concentration of SA or MSA ranges between 10^5 and 10^9 molecules cm^{-3} , the formation rates of (MGA)(SA) and (MGA)(MSA) are in the ranges of 10^0 to 10^4 $\text{cm}^{-3} \text{s}^{-1}$ and 10^{-1} to 10^3 $\text{cm}^{-3} \text{s}^{-1}$, respectively. At 208 K, when the concentration of SA or MSA varies from 10^5 to 10^9 molecules cm^{-3} , the formation rates of (MGA)(SA) and (MGA)(MSA) vary from 10^3 to 10^7 $\text{cm}^{-3} \text{s}^{-1}$ and from 10^2 to 10^6 $\text{cm}^{-3} \text{s}^{-1}$, respectively. The formation rates at 208 K are 10^3 times as high as those at 248 K, which shows the same kind of temperature dependence as the experiments of Dunne et al.¹²⁴ In their experiments on SA–ammonia, the nucleation rates at 208 K were 10^4 times as high as those at 248 K.

Furthermore, we set the MGA concentration to 10 pptv and the concentration of SA or MSA to 10^7 molecules cm^{-3} to investigate the formation rates of (MGA)_i(SA)_j ($i = 1-2, j = 1-2$) and (MGA)_i(MSA)_j ($i = 1-2, j = 1-2$) at 298.15 K. As listed in Table S3 in the Supporting Information, for MGA–SA, the formation rates of (MGA)(SA), (MGA)(SA)₂, (MGA)₂(SA), and (MGA)₂(SA)₂ were 3.71×10^{-1} , 1.15×10^{-8} , 6.51×10^{-8} , and 8.58×10^{-16} $\text{cm}^{-3} \text{s}^{-1}$, respectively. For MGA–MSA, the formation rates of (MGA)(MSA), (MGA)(MSA)₂, (MGA)₂(MSA), and (MGA)₂(MSA)₂ at 298.15 K were 3.60×10^{-2} , 4.53×10^{-10} , 3.55×10^{-10} , and 1.03×10^{-19} $\text{cm}^{-3} \text{s}^{-1}$, respectively. For both the MGA–SA and MGA–MSA systems, the formation rate of the heterodimer was the highest.

In general, MGA–SA and MGA–MSA clusters contribute to NPF mainly in the form of the heterodimer. The formation rates of MGA–SA clusters are higher than those of MGA–

MSA clusters, which indicates that, in the atmosphere, MGA is easier to nucleate with SA than MSA is, which is consistent with the above analysis of evaporation rates.

4. CONCLUSIONS

The structures, thermodynamic properties, evaporation rates, and formation rates of (MGA)_i(SA)_j ($i = 1-2, j = 1-2$) and (MGA)_i(MSA)_j ($i = 1-2, j = 1-2$) clusters were analyzed. The (MGA)(SA)_m ($m = 1-2$) and (MGA)(MSA)_n ($n = 1-2$) clusters have favorable and comparable Gibbs free energies, binding energies, and formation enthalpies. The (MGA)(SA) and (MGA)(MSA) clusters are the most stable clusters in the given MGA–SA and MGA–MSA systems, respectively, and the formation rates of them are quite large, suggesting that both the (MGA)(SA) and (MGA)(MSA) clusters could have significant contributions to NPF events.

Our theoretical studies show that the heteromolecular nucleation between MGA and SA or MSA could play an important role in nucleation events, which is consistent with the previous HOMs experimental results. The temperature dependence of formation rates and total evaporation rates indicates that the lower the temperature, the lower the total evaporation rates and the higher the formation rates, which corresponds to the phenomenon that haze in winter is more serious than in summer. The nucleation ability of the MGA–MSA system is slightly weaker than that of the MGA–SA system, which may rely on the fact that the acidity of SA is stronger than that of MSA. Our results provide a theoretical basis for understanding the nucleation mechanism involving HOMs. Taking the complexity of the atmospheric environment into account, further research on MGA–SA and MGA–MSA systems could be extended to ternary systems such as MGA–SA–amine and MGA–MSA–amine.

■ ASSOCIATED CONTENT

Supporting Information

The Supporting Information is available free of charge on the ACS Publications website at DOI: 10.1021/acs.jpca.9b03142.

Benchmarks of the DF-MP2-F12/VDZ-F12 theory level, the structures of the clusters containing two MGA molecules, the Cartesian coordinates of all structures optimized at M06-2X/6-311++G(3df,3pd) theory level, the formation entropies and enthalpies of clusters obtained at DF-MP2-F12/VDZ-F12//M06-2X/6-311++G(3df,3pd) theory level, and the formation rates and

total evaporation rates of clusters obtained by atmospheric dynamics simulation at 298.15 K (PDF)

AUTHOR INFORMATION

Corresponding Authors

*E-mail: fengyj6@ustc.edu.cn (Y.-J.F.).

*E-mail: huangwei6@ustc.edu.cn (W.H.).

ORCID

Wei Huang: 0000-0001-8147-386X

Notes

The authors declare no competing financial interest.

ACKNOWLEDGMENTS

This work was supported by the National Natural Science Foundation of China (grant nos. 41775122, 21573241, 41605099, 41705097, 41705111, 41775112, and 41527808), the National Science Fund for Distinguished Young Scholars (grant no. 41725019), Key Research Program of Frontier Science, CAS (grant no. QYZDB-SSW-DQC031), The Key Research Program of the Chinese Academy of Sciences (grant no. ZDRW-ZS-2016-4-3-6), the National Key Research and Development program (grant no. 2016YFC0202203 and 2016YFC0202703), National Research Program for Key Issues in Air Pollution Control (grant no. DQGG0103), and the Fundamental Research Funds for the Central Universities (grant no. WK2100100031).

REFERENCES

- (1) Cao, C.; Jiang, W.; Wang, B.; Fang, J.; Lang, J.; Tian, G.; Jiang, J.; Zhu, T. F. Inhalable Microorganisms in Beijing's PM_{2.5} and PM₁₀ Pollutants during a Severe Smog Event. *Environ. Sci. Technol.* **2014**, *48*, 1499–1507.
- (2) Charlson, R. J.; Schwartz, S. E.; Hales, J. M.; Cess, R. D.; Coakley, J. A.; Hansen, J. E.; Hofmann, D. J. Climate forcing by anthropogenic aerosols. *Science* **1992**, *255*, 423–430.
- (3) Kulmala, M.; Vehkamäki, H.; Petäjä, T.; Dal Maso, M.; Lauri, A.; Kerminen, V.-M.; Birmili, W.; McMurry, P. H. Formation and growth rates of ultrafine atmospheric particles: a review of observations. *J. Aerosol Sci.* **2004**, *35*, 143–176.
- (4) Zhang, R.; Li, G.; Fan, J.; Wu, D. L.; Molina, M. J. Intensification of pacific storm track linked to Asian pollution. *Proc. Natl. Acad. Sci. U.S.A.* **2007**, *104*, S295–S299.
- (5) Oberdörster, G.; Utell, M. J. Ultrafine particles in the urban air: to the respiratory tract—and beyond? *Environ. Health Perspect.* **2002**, *110*, A440–A441.
- (6) Haywood, J.; Boucher, O. Estimates of the direct and indirect radiative forcing due to tropospheric aerosols: A review. *Rev. Geophys.* **2000**, *38*, 513–543.
- (7) Wang, L.; Khalizov, A. F.; Zheng, J.; Xu, W.; Ma, Y.; Lal, V.; Zhang, R. Atmospheric nanoparticles formed from heterogeneous reactions of organics. *Nat. Geosci.* **2010**, *3*, 238–242.
- (8) Zhang, R. Getting to the critical nucleus of aerosol formation. *Science* **2010**, *328*, 1366–1367.
- (9) Zhang, R.; Khalizov, A.; Wang, L.; Hu, M.; Xu, W. Nucleation and growth of nanoparticles in the atmosphere. *Chem. Rev.* **2011**, *112*, 1957–2011.
- (10) Kulmala, M. ATMOSPHERIC SCIENCE: How Particles Nucleate and Grow. *Science* **2003**, *302*, 1000–1001.
- (11) Kulmala, M.; Kontkanen, J.; Junninen, H.; Lehtipalo, K.; Manninen, H. E.; Nieminen, T.; Petaja, T.; Sipilä, M.; Schobesberger, S.; Rantala, P.; et al. Direct observations of atmospheric aerosol nucleation. *Science* **2013**, *339*, 943–946.
- (12) Kulmala, M.; Petäjä, T.; Nieminen, T.; Sipilä, M.; Manninen, H. E.; Lehtipalo, K.; Dal Maso, M.; Aalto, P. P.; Junninen, H.; Paasonen, P.; et al. Measurement of the nucleation of atmospheric aerosol particles. *Nat. Protoc.* **2012**, *7*, 1651–1667.
- (13) Zhang, R.; Suh, I.; Zhao, J.; Zhang, D.; Fortner, E. C.; Tie, X.; Molina, L. T.; Molina, M. J. Atmospheric new particle formation enhanced by organic acids. *Science* **2004**, *304*, 1487–1490.
- (14) Henschel, H.; Kurtén, T.; Vehkamäki, H. Computational study on the effect of hydration on new particle formation in the sulfuric acid/ammonia and sulfuric acid/dimethylamine systems. *J. Phys. Chem. A* **2016**, *120*, 1886–1896.
- (15) Elm, J.; Jen, C. N.; Kurtén, T.; Vehkamäki, H. Strong hydrogen bonded molecular interactions between atmospheric diamines and sulfuric acid. *J. Phys. Chem. A* **2016**, *120*, 3693–3700.
- (16) Aalto, P.; Hämeri, K.; Becker, E.; Weber, R.; Salm, J.; Mäkelä, J. M.; Hoell, C.; O’Dowd, C. D.; Hansson, H.-C.; Väkevä, M.; et al. Physical characterization of aerosol particles during nucleation events. *Tellus B* **2001**, *53*, 344–358.
- (17) O’Dowd, C.; McFiggans, G.; Creasey, D. J.; Pirjola, L.; Hoell, C.; Smith, M. H.; Allan, B. J.; Plane, J. M. C.; Heard, D. E.; Lee, J. D.; et al. On the photochemical production of new particles in the coastal boundary layer. *Geophys. Res. Lett.* **1999**, *26*, 1707–1710.
- (18) Andreae, M. O. The aerosol nucleation puzzle. *Science* **2013**, *339*, 911–912.
- (19) Metzger, A.; Verheggen, B.; Dommen, J.; Duplissy, J.; Prevot, A. S. H.; Weingartner, E.; Riipinen, I.; Kulmala, M.; Spracklen, D. V.; Carslaw, K. S.; et al. Evidence for the role of organics in aerosol particle formation under atmospheric conditions. *Proc. Natl. Acad. Sci. U.S.A.* **2010**, *107*, 6646–6651.
- (20) Zhang, R.; Wang, L.; Khalizov, A. F.; Zhao, J.; Zheng, J.; McGraw, R. L.; Molina, L. T. Formation of nanoparticles of blue haze enhanced by anthropogenic pollution. *Proc. Natl. Acad. Sci. U.S.A.* **2009**, *106*, 17650–17654.
- (21) Zhao, J.; Khalizov, A.; Zhang, R.; McGraw, R. Hydrogen-bonding interaction in molecular complexes and clusters of aerosol nucleation precursors. *J. Phys. Chem. A* **2009**, *113*, 680–689.
- (22) Ehn, M.; Thornton, J. A.; Kleist, E.; Sipilä, M.; Junninen, H.; Pullinen, I.; Springer, M.; Rubach, F.; Tillmann, R.; Lee, B.; et al. A large source of low-volatility secondary organic aerosol. *Nature* **2014**, *506*, 476–479.
- (23) Riccobono, F.; Schobesberger, S.; Scott, C. E.; Dommen, J.; Ortega, I. K.; Rondo, L.; Almeida, J.; Amorim, A.; Bianchi, F.; Breitenlechner, M.; et al. Oxidation products of biogenic emissions contribute to nucleation of atmospheric particles. *Science* **2014**, *344*, 717–721.
- (24) Donahue, N. M.; Ortega, I. K.; Chuang, W.; Riipinen, I.; Riccobono, F.; Schobesberger, S.; Dommen, J.; Baltensperger, U.; Kulmala, M.; Worsnop, D. R.; et al. How do organic vapors contribute to new-particle formation? *Faraday Discuss.* **2013**, *165*, 91–104.
- (25) Cappa, C. Atmospheric science: Unexpected player in particle formation. *Nature* **2016**, *533*, 478–479.
- (26) Bianchi, F.; Trostl, J.; Junninen, H.; Frege, C.; Henne, S.; Hoyle, C. R.; Molteni, U.; Herrmann, E.; Adamov, A.; Bukowiecki, N.; et al. New particle formation in the free troposphere: A question of chemistry and timing. *Science* **2016**, *352*, 1109–1112.
- (27) Lehtipalo, K.; Yan, C.; Dada, L.; Bianchi, F.; Xiao, M.; Wagner, R.; Stolzenburg, D.; Ahonen, L. R.; Amorim, A.; Baccharini, A.; et al. Multicomponent new particle formation from sulfuric acid, ammonia, and biogenic vapors. *Sci Adv* **2018**, *4*, No. eaau5363.
- (28) Tröstl, J.; Chuang, W. K.; Gordon, H.; Heinritzi, M.; Yan, C.; Molteni, U.; Ahlm, L.; Frege, C.; Bianchi, F.; Wagner, R.; et al. The role of low-volatility organic compounds in initial particle growth in the atmosphere. *Nature* **2016**, *533*, 527–531.
- (29) Kirkby, J.; Duplissy, J.; Sengupta, K.; Frege, C.; Gordon, H.; Williamson, C.; Heinritzi, M.; Simon, M.; Yan, C.; Almeida, J.; et al. Ion-induced nucleation of pure biogenic particles. *Nature* **2016**, *533*, 521–526.
- (30) Bianchi, F.; Kurtén, T.; Riva, M.; Mohr, C.; Rissanen, M. P.; Roldin, P.; Berndt, T.; Crouse, J. D.; Wennberg, P. O.; Mentel, T. F.; et al. Highly oxygenated organic molecules (HOM) from gas-phase

autoxidation involving peroxy radicals: a key contributor to atmospheric aerosol. *Chem. Rev.* **2019**, *119*, 3472–3509.

(31) Kulmala, M.; Petäjä, T.; Ehn, M.; Thornton, J.; Sipilä, M.; Worsnop, D. R.; Kerminen, V.-M. Chemistry of atmospheric nucleation: on the recent advances on precursor characterization and atmospheric cluster composition in connection with atmospheric new particle formation. *Annu. Rev. Phys. Chem.* **2014**, *65*, 21–37.

(32) Qi, X.; Ding, A.; Roldin, P.; Xu, Z.; Zhou, P.; Sarnela, N.; Nie, W.; Huang, X.; Rusanen, A.; Ehn, M.; et al. Modelling studies of HOMs and their contributions to new particle formation and growth: comparison of boreal forest in Finland and a polluted environment in China. *Atmos. Chem. Phys.* **2018**, *18*, 11779–11791.

(33) Rose, C.; Zha, Q.; Dada, L.; Yan, C.; Lehtipalo, K.; Junninen, H.; Mazon, S. B.; Jokinen, T.; Sarnela, N.; Sipilä, M.; et al. Observations of biogenic ion-induced cluster formation in the atmosphere. *Sci. Adv.* **2018**, *4*, No. eaar5218.

(34) Yu, F.; Luo, G.; Pryor, S. C.; Pillai, P. R.; Lee, S. H.; Ortega, J.; Schwab, J. J.; Hallar, A. G.; Leaitch, W. R.; Aneja, V. P.; et al. Spring and summer contrast in new particle formation over nine forest areas in North America. *Atmos. Chem. Phys.* **2015**, *15*, 13993–14003.

(35) Turpin, B. J.; Huntzicker, J. J. Identification of secondary organic aerosol episodes and quantitation of primary and secondary organic aerosol concentrations during SCAQS. *Atmos. Environ.* **1995**, *29*, 3527–3544.

(36) Turpin, B. J.; Lim, H.-J. Species Contributions to PM_{2.5} Mass Concentrations: Revisiting Common Assumptions for Estimating Organic Mass. *Aerosol Sci. Technol.* **2001**, *35*, 602–610.

(37) Cabada, J. C.; Pandis, S. N.; Robinson, A. L. Sources of atmospheric carbonaceous particulate matter in Pittsburgh, Pennsylvania. *J. Air Waste Manage. Assoc.* **2002**, *52*, 732–741.

(38) Guenther, A.; Hewitt, C. N.; Erickson, D.; Fall, R.; Geron, C.; Graedel, T.; Harley, P.; Klinger, L.; Lerdau, M.; McKay, W. A.; et al. A global model of natural volatile organic compound emissions. *J. Geophys. Res.: Atmos.* **1995**, *100*, 8873–8892.

(39) Guenther, A.; Karl, T.; Harley, P.; Wiedinmyer, C.; Palmer, P. I.; Geron, C. Estimates of global terrestrial isoprene emissions using MEGAN (Model of Emissions of Gases and Aerosols from Nature). *Atmos. Chem. Phys.* **2006**, *6*, 3181–3210.

(40) Claeys, M.; Graham, B.; Vas, G.; Wang, W.; Vermeylen, R.; Pashynska, V.; Cafmeyer, J.; Guyon, P.; Andreae, M. O.; Artaxo, P.; et al. Formation of secondary organic aerosols through photooxidation of isoprene. *Science* **2004**, *303*, 1173–1176.

(41) Xu, L.; Guo, H.; Boyd, C. M.; Klein, M.; Bougiatioti, A.; Cerully, K. M.; Hite, J. R.; Isaacman-VanWertz, G.; Kreisberg, N. M.; Knote, C.; et al. Effects of anthropogenic emissions on aerosol formation from isoprene and monoterpenes in the southeastern United States. *Proc. Natl. Acad. Sci. U.S.A.* **2015**, *112*, 37–42.

(42) Henze, D. K.; Seinfeld, J. H. Global secondary organic aerosol from isoprene oxidation. *Geophys. Res. Lett.* **2006**, *33*, L09812.

(43) Hoyle, C. R.; Berntsen, T.; Myhre, G.; Isaksen, I. S. A. Secondary organic aerosol in the global aerosol–chemical transport model Oslo CTM2. *Atmos. Chem. Phys.* **2007**, *7*, 5675–5694.

(44) Edney, E. O.; Kleindienst, T. E.; Jaoui, M.; Lewandowski, M.; Offenberg, J. H.; Wang, W.; Claeys, M. Formation of 2-methyl tetrols and 2-methylglyceric acid in secondary organic aerosol from laboratory irradiated isoprene/NO_x/SO₂/air mixtures and their detection in ambient PM_{2.5} samples collected in the eastern United States. *Atmos. Environ.* **2005**, *39*, 5281–5289.

(45) Surratt, J. D.; Murphy, S. M.; Kroll, J. H.; Ng, N. L.; Hildebrandt, L.; Sorooshian, A.; Szmigielski, R.; Vermeylen, R.; Maenhaut, W.; Claeys, M.; et al. Chemical composition of secondary organic aerosol formed from the photooxidation of isoprene. *J. Phys. Chem. A* **2006**, *110*, 9665–9690.

(46) Ion, A. C.; Vermeylen, R.; Kourtev, I.; Cafmeyer, J.; Chi, X.; Gelencsér, A.; Maenhaut, W.; Claeys, M. Polar organic compounds in rural PM_{2.5} aerosols from K-pusztá, Hungary, during a 2003 summer field campaign: Sources and diel variations. *Atmos. Chem. Phys.* **2005**, *5*, 1805–1814.

(47) Jaoui, M.; Corse, E. W.; Lewandowski, M.; Offenberg, J. H.; Kleindienst, T. E.; Edney, E. O. Formation of organic tracers for isoprene SOA under acidic conditions. *Atmos. Environ.* **2010**, *44*, 1798–1805.

(48) Szmigielski, R.; Surratt, J. D.; Vermeylen, R.; Szmigielska, K.; Kroll, J. H.; Ng, N. L.; Murphy, S. M.; Sorooshian, A.; Seinfeld, J. H.; Claeys, M. Characterization of 2-methylglyceric acid oligomers in secondary organic aerosol formed from the photooxidation of isoprene using trimethylsilylation and gas chromatography/ion trap mass spectrometry. *J. Mass Spectrom.* **2007**, *42*, 101–116.

(49) Kleindienst, T. E.; Jaoui, M.; Lewandowski, M.; Offenberg, J. H.; Lewis, C. W.; Bhave, P. V.; Edney, E. O. Estimates of the contributions of biogenic and anthropogenic hydrocarbons to secondary organic aerosol at a southeastern US location. *Atmos. Environ.* **2007**, *41*, 8288–8300.

(50) Zhang, H.; Surratt, J. D.; Lin, Y. H.; Bapat, J.; Kamens, R. M. Effect of relative humidity on SOA formation from isoprene/NO photooxidation: enhancement of 2-methylglyceric acid and its corresponding oligoesters under dry conditions. *Atmos. Chem. Phys.* **2011**, *11*, 6411–6424.

(51) Nestorowicz, K.; Jaoui, M.; Rudzinski, K. J.; Lewandowski, M.; Kleindienst, T. E.; Spólnik, G.; Danikiewicz, W.; Szmigielski, R. Chemical composition of isoprene SOA under acidic and non-acidic conditions: effect of relative humidity. *Atmos. Chem. Phys.* **2018**, *18*, 18101–18121.

(52) Nguyen, T. B.; Laskin, J.; Laskin, A.; Nizkorodov, S. A. Nitrogen-containing organic compounds and oligomers in secondary organic aerosol formed by photooxidation of isoprene. *Environ. Sci. Technol.* **2011**, *45*, 6908–6918.

(53) Li, J.; Wang, G.; Wu, C.; Cao, C.; Ren, Y.; Wang, J.; Li, J.; Cao, J.; Zeng, L.; Zhu, T. Characterization of isoprene-derived secondary organic aerosols at a rural site in North China Plain with implications for anthropogenic pollution effects. *Sci. Rep.* **2018**, *8*, 535.

(54) Hong, Z.; Zhang, H.; Zhang, Y.; Xu, L.; Liu, T.; Xiao, H.; Hong, Y.; Chen, J.; Li, M.; Deng, J.; et al. Secondary organic aerosol of PM_{2.5} in a mountainous forest area in southeastern China: Molecular compositions and tracers implication. *Sci. Total Environ.* **2019**, *653*, 496–503.

(55) Ding, X.; Wang, X.; Xie, Z.; Zhang, Z.; Sun, L. Impacts of Siberian biomass burning on organic aerosols over the North Pacific Ocean and the Arctic: Primary and secondary organic tracers. *Environ. Sci. Technol.* **2013**, *47*, 3149–3157.

(56) Guo, T.; Guo, Z. Impacts of biomass burning on organic aerosols over the Northwestern Pacific Ocean. *AGU Fall Meeting Abstracts*, 2017.

(57) Hu, Q.-H.; Xie, Z.-Q.; Wang, X.-M.; Kang, H.; He, Q.-F.; Zhang, P. Secondary organic aerosols over oceans via oxidation of isoprene and monoterpenes from Arctic to Antarctic. *Sci. Rep.* **2013**, *3*, 2280.

(58) Kang, M.; Fu, P.; Kawamura, K.; Yang, F.; Zhang, H.; Zang, Z.; Ren, H.; Ren, L.; Zhao, Y.; Sun, Y.; et al. Characterization of biogenic primary and secondary organic aerosols in the marine atmosphere over the East China Sea. *Atmos. Chem. Phys.* **2018**, *18*, 13947–13967.

(59) Pokhrel, A.; Kawamura, K.; Ono, K.; Seki, O.; Fu, P.; Matoba, S.; Shiraiwa, T. Ice core records of monoterpene- and isoprene-SOA tracers from Aurora Peak in Alaska since 1660s: Implication for climate change variability in the North Pacific Rim. *Atmos. Environ.* **2016**, *130*, 105–112.

(60) Fu, P.; Kawamura, K.; Miura, K. Molecular characterization of marine organic aerosols collected during a round-the-world cruise. *J. Geophys. Res.: Atmos.* **2011**, *116*, D13302.

(61) Fu, P. Q.; Kawamura, K.; Chen, J.; Charrière, B.; Sempéré, R. Organic molecular composition of marine aerosols over the Arctic Ocean in summer: contributions of primary emission and secondary aerosol formation. *Biogeosciences* **2013**, *10*, 653–667.

(62) Barnes, I.; Hjorth, J.; Mihalopoulos, N. Dimethyl sulfide and dimethyl sulfoxide and their oxidation in the atmosphere. *Chem. Rev.* **2006**, *106*, 940–975.

- (63) Glasow, R. v.; Crutzen, P. Model study of multiphase DMS oxidation with a focus on halogens. *Atmos. Chem. Phys.* **2004**, *4*, 589–608.
- (64) Berresheim, H.; Eisele, F. L.; Tanner, D. J.; McInnes, L. M.; Ramsey-Bell, D. C.; Covert, D. S. Atmospheric sulfur chemistry and cloud condensation nuclei (CCN) concentrations over the northeastern Pacific coast. *J. Geophys. Res.: Atmos.* **1993**, *98*, 12701–12711.
- (65) Berresheim, H.; Elste, T.; Tremmel, H. G.; Allen, A. G.; Hansson, H. C.; Rosman, K.; Dal Maso, M.; Mäkelä, J. M.; Kulmala, M.; O'Dowd, C. D. Gas–aerosol relationships of H₂SO₄, MSA, and OH: Observations in the coastal marine boundary layer at Mace Head, Ireland. *J. Geophys. Res.: Atmos.* **2002**, *107*, 8100.
- (66) Mauldin, R. L.; Tanner, D. J.; Heath, J. A.; Huebert, B. J.; Eisele, F. L. Observations of H₂SO₄ and MSA during PEM-Tropics-A. *J. Geophys. Res.: Atmos.* **1999**, *104*, 5801–5816.
- (67) Mauldin, R. L., III; Cantrell, C. A.; Zondlo, M.; Kosciuch, E.; Eisele, F. L.; Chen, G.; Davis, D.; Weber, R.; Crawford, J.; Blake, D.; et al. Measurements of OH, H₂SO₄, and MSA during tropospheric ozone production about the spring equinox (TOPSE). *J. Geophys. Res.: Atmos.* **2003**, *108*, 8796.
- (68) Wyslouzil, B. E.; Seinfeld, J. H.; Flagan, R. C.; Okuyama, K. Binary nucleation in acid-water systems. I. Methanesulfonic acid-water. *J. Chem. Phys.* **1991**, *94*, 6827–6841.
- (69) Wyslouzil, B. E.; Seinfeld, J. H.; Flagan, R. C.; Okuyama, K. Binary nucleation in acid-water systems. II. Sulfuric acid-water and a comparison with methanesulfonic acid-water. *J. Chem. Phys.* **1991**, *94*, 6842–6850.
- (70) Dall'Osto, M.; Ceburnis, D.; Monahan, C.; Worsnop, D. R.; Bialek, J.; Kulmala, M.; Kurtén, T.; Ehn, M.; Wenger, J.; Sodeau, J.; et al. Nitrogenated and aliphatic organic vapors as possible drivers for marine secondary organic aerosol growth. *J. Geophys. Res.: Atmos.* **2012**, *117*, D12311.
- (71) Ezell, M. J.; Chen, H.; Arquero, K. D.; Finlayson-Pitts, B. J. Aerosol fast flow reactor for laboratory studies of new particle formation. *J. Aerosol Sci.* **2014**, *78*, 30–40.
- (72) Dawson, M. L.; Varner, M. E.; Perraud, V.; Ezell, M. J.; Gerber, R. B.; Finlayson-Pitts, B. J. Simplified mechanism for new particle formation from methanesulfonic acid, amines, and water via experiments and ab initio calculations. *Proc. Natl. Acad. Sci. U.S.A.* **2012**, *109*, 18719–18724.
- (73) Dawson, M. L.; Varner, M. E.; Perraud, V.; Ezell, M. J.; Wilson, J.; Zelenyuk, A.; Gerber, R. B.; Finlayson-Pitts, B. J. Amine-Amine Exchange in Aminium-Methanesulfonate Aerosols. *J. Phys. Chem. C* **2014**, *118*, 29431–29440.
- (74) Nishino, N.; Arquero, K. D.; Dawson, M. L.; Finlayson-Pitts, B. J. Infrared studies of the reaction of methanesulfonic acid with trimethylamine on surfaces. *Environ. Sci. Technol.* **2013**, *48*, 323–330.
- (75) Chen, H.; Ezell, M. J.; Arquero, K. D.; Varner, M. E.; Dawson, M. L.; Gerber, R. B.; Finlayson-Pitts, B. J. New particle formation and growth from methanesulfonic acid, trimethylamine and water. *Phys. Chem. Chem. Phys.* **2015**, *17*, 13699–13709.
- (76) Chen, H.; Varner, M. E.; Gerber, R. B.; Finlayson-Pitts, B. J. Reactions of methanesulfonic acid with amines and ammonia as a source of new particles in air. *J. Phys. Chem. B* **2015**, *120*, 1526–1536.
- (77) Facchini, M. C.; Decesari, S.; Rinaldi, M.; Carbone, C.; Finessi, E.; Mircea, M.; Fuzzi, S.; Moretti, F.; Tagliavini, E.; Ceburnis, D.; et al. Important source of marine secondary organic aerosol from biogenic amines. *Environ. Sci. Technol.* **2008**, *42*, 9116–9121.
- (78) Arquero, K. D. The effect of organics on particle formation and growth from methanesulfonic acid, amines and water. Doctoral Dissertation, UC Irvine, 2017.
- (79) Schobesberger, S.; Junninen, H.; Bianchi, F.; Lonn, G.; Ehn, M.; Lehtipalo, K.; Dommen, J.; Ehrhart, S.; Ortega, I. K.; Franchin, A.; et al. Molecular understanding of atmospheric particle formation from sulfuric acid and large oxidized organic molecules. *Proc. Natl. Acad. Sci. U.S.A.* **2013**, *110*, 17223–17228.
- (80) Wales, D. J.; Doye, J. P. K. Global optimization by basin-hopping and the lowest energy structures of Lennard-Jones clusters containing up to 110 atoms. *J. Phys. Chem. A* **1997**, *101*, 5111–5116.
- (81) Huang, W.; Pal, R.; Wang, L.-M.; Zeng, X. C.; Wang, L.-S. Isomer identification and resolution in small gold clusters. *J. Chem. Phys.* **2010**, *132*, 054305.
- (82) Hostaš, J.; Režáč, J.; Hobza, P. On the performance of the semiempirical quantum mechanical PM6 and PM7 methods for noncovalent interactions. *Chem. Phys. Lett.* **2013**, *568*, 161–166.
- (83) Maia, J. D. C.; Urquiza Carvalho, G. A.; Manguiera, C. P., Jr; Santana, S. R.; Cabral, L. A. F.; Rocha, G. B. GPU linear algebra libraries and GPGPU programming for accelerating MOPAC semiempirical quantum chemistry calculations. *J. Chem. Theory Comput.* **2012**, *8*, 3072–3081.
- (84) Elm, J.; Bilde, M.; Mikkelsen, K. V. Assessment of density functional theory in predicting structures and free energies of reaction of atmospheric prenucleation clusters. *J. Chem. Theory Comput.* **2012**, *8*, 2071–2077.
- (85) Bork, N.; Du, L.; Reiman, H.; Kurtén, T.; Kjaergaard, H. G. Benchmarking ab initio binding energies of hydrogen-bonded molecular clusters based on FTIR spectroscopy. *J. Phys. Chem. A* **2014**, *118*, 5316–5322.
- (86) Zhao, Y.; Truhlar, D. G. The M06 suite of density functionals for main group thermochemistry, thermochemical kinetics, non-covalent interactions, excited states, and transition elements: two new functionals and systematic testing of four M06-class functionals and 12 other functionals. *Theor. Chem. Acc.* **2008**, *120*, 215–241.
- (87) Liu, L.; Zhang, X.; Li, Z.; Zhang, Y.; Ge, M. Gas-phase hydration of glyoxylic acid: Kinetics and atmospheric implications. *Chemosphere* **2017**, *186*, 430–437.
- (88) Elm, J.; Kristensen, K. Basis set convergence of the binding energies of strongly hydrogen-bonded atmospheric clusters. *Phys. Chem. Chem. Phys.* **2017**, *19*, 1122–1133.
- (89) Ge, P.; Luo, G.; Luo, Y.; Huang, W.; Xie, H.; Chen, J.; Qu, J. Molecular understanding of the interaction of amino acids with sulfuric acid in the presence of water and the atmospheric implication. *Chemosphere* **2018**, *210*, 215–223.
- (90) Frisch, M.; Trucks, G.; Schlegel, H. B.; Scuseria, G. E.; Robb, M. A.; Cheeseman, J. R.; Scalmani, G.; Barone, V.; Mennucci, B.; Petersson, G., et al. *Gaussian 09*, Revision D. 01; Gaussian, Inc.: Wallingford, CT, 2009.
- (91) Werner, H.-J.; Adler, T. B.; Manby, F. R. General orbital invariant MP2-F12 theory. *J. Chem. Phys.* **2007**, *126*, 164102.
- (92) Werner, H.; Knowles, P.; Knizia, G.; Manby, F.; Schütz, M.; Celani, P.; Korona, T.; Lindh, R.; Mitrushenkov, A.; Rauhut, G., et al. *MOLPRO*, version 2010.1, a package of ab initio programs; see <http://www.molpro.net>.
- (93) Werner, H.-J.; Knowles, P. J.; Knizia, G.; Manby, F. R.; Schütz, M. Molpro: a general-purpose quantum chemistry program package. *Wiley Interdiscip. Rev.: Comput. Mol. Sci.* **2012**, *2*, 242–253.
- (94) McGrath, M. J.; Olenius, T.; Ortega, I. K.; Loukonen, V.; Paasonen, P.; Kurtén, T.; Kulmala, M.; Vehkamäki, H. Atmospheric Cluster Dynamics Code: a flexible method for solution of the birth-death equations. *Atmos. Chem. Phys.* **2012**, *12*, 2345–2355.
- (95) Kontkanen, J.; Olenius, T.; Kulmala, M.; Riipinen, I. Exploring the potential of nano-Köhler theory to describe the growth of atmospheric molecular clusters by organic vapors using cluster kinetics simulations. *Atmos. Chem. Phys.* **2018**, *18*, 13733–13754.
- (96) Li, H.; Kupiainen-Määttä, O.; Zhang, H.; Zhang, X.; Ge, M. A molecular-scale study on the role of lactic acid in new particle formation: Influence of relative humidity and temperature. *Atmos. Environ.* **2017**, *166*, 479–487.
- (97) Zhang, H.; Li, H.; Liu, L.; Zhang, Y.; Zhang, X.; Li, Z. The potential role of malonic acid in the atmospheric sulfuric acid–Ammonia clusters formation. *Chemosphere* **2018**, *203*, 26–33.
- (98) Zhang, H.; Wang, W.; Pi, S.; Liu, L.; Li, H.; Chen, Y.; Zhang, Y.; Zhang, X.; Li, Z. Gas phase transformation from organic acid to organic sulfuric anhydride: Possibility and atmospheric fate in the initial new particle formation. *Chemosphere* **2018**, *212*, 504–512.
- (99) Bader, R. *Atoms in Molecules: A Quantum Theory*; Clarendon: Oxford, UK, 1990.

- (100) Carroll, M. T.; Chang, C.; Bader, R. F. W. Prediction of the structures of hydrogen-bonded complexes using the Laplacian of the charge density. *Mol. Phys.* **1988**, *63*, 387–405.
- (101) Gao, W.; Jiao, J.; Feng, H.; Xuan, X.; Chen, L. Natures of benzene-water and pyrrole-water interactions in the forms of σ and π types: theoretical studies from clusters to liquid mixture. *J. Mol. Model.* **2013**, *19*, 1273–1283.
- (102) Bone, R. G. A.; Bader, R. F. W. Identifying and Analyzing Intermolecular Bonding Interactions in van der Waals Molecules. *J. Phys. Chem.* **1996**, *100*, 10892–10911.
- (103) Rozas, I.; Alkorta, I.; Elguero, J. Behavior of ylides containing N, O, and C atoms as hydrogen bond acceptors. *J. Am. Chem. Soc.* **2000**, *122*, 11154–11161.
- (104) Lu, T. *Multiwfn Program*, version 3.5., 2018; see <http://sobereva.com/multiwfn/>.
- (105) Koch, U.; Popelier, P. L. A. Characterization of C-H-O Hydrogen Bonds on the Basis of the Charge Density. *J. Phys. Chem.* **1995**, *99*, 9747–9754.
- (106) Gilli, P.; Bertolasi, V.; Ferretti, V.; Gilli, G. Evidence for resonance-assisted hydrogen bonding. 4. Covalent nature of the strong homonuclear hydrogen bond. Study of the O-H-O system by crystal structure correlation methods. *J. Am. Chem. Soc.* **1994**, *116*, 909–915.
- (107) Gilli, G.; Gilli, P. Towards a unified hydrogen-bond theory. *J. Mol. Struct.* **2000**, *552*, 1–15.
- (108) Gilli, P.; Bertolasi, V.; Pretto, L.; Gilli, G. Outline of a transition-state hydrogen-bond theory. *J. Mol. Struct.* **2006**, *790*, 40–49.
- (109) Gilli, P.; Gilli, G. Hydrogen bond models and theories: The dual hydrogen bond model and its consequences. *J. Mol. Struct.* **2010**, *972*, 2–10.
- (110) Johnson, E. R.; Keinan, S.; Mori-Sánchez, P.; Contreras-García, J.; Cohen, A. J.; Yang, W. Revealing noncovalent interactions. *J. Am. Chem. Soc.* **2010**, *132*, 6498–6506.
- (111) Contreras-García, J.; Yang, W.; Johnson, E. R. Analysis of hydrogen-bond interaction potentials from the electron density: integration of noncovalent interaction regions. *J. Phys. Chem. A* **2011**, *115*, 12983–12990.
- (112) Hohenberg, P.; Kohn, W. Inhomogeneous electron gas. *Phys. Rev.* **1964**, *136*, B864.
- (113) Cohen, A. J.; Mori-Sánchez, P.; Yang, W. Insights into current limitations of density functional theory. *Science* **2008**, *321*, 792–794.
- (114) Humphrey, W.; Dalke, A.; Schulten, K. VMD: visual molecular dynamics. *J. Mol. Graphics* **1996**, *14*, 33–38.
- (115) Jiang, S.; Huang, T.; Liu, Y.-R.; Xu, K.-M.; Zhang, Y.; Lv, Y.-Z.; Huang, W. Theoretical study of temperature dependence and Rayleigh scattering properties of chloride hydration clusters. *Phys. Chem. Chem. Phys.* **2014**, *16*, 19241–19249.
- (116) Mhin, B. J.; Lee, S. J.; Kim, K. S. Water-cluster distribution with respect to pressure and temperature in the gas phase. *Phys. Rev. A* **1993**, *48*, 3764.
- (117) Kim, J.; Mhin, B. J.; Lee, S. J.; Kim, K. S. Entropy-driven structures of the water octamer. *Chem. Phys. Lett.* **1994**, *219*, 243–246.
- (118) Lee, H. M.; Suh, S. B.; Lee, J. Y.; Tarakeshwar, P.; Kim, K. S. Structures, energies, vibrational spectra, and electronic properties of water monomer to decamer. *J. Chem. Phys.* **2000**, *112*, 9759–9772.
- (119) Ortega, I. K.; Kupiainen, O.; Kurtén, T.; Olenius, T.; Wilkman, O.; McGrath, M. J.; Loukonen, V.; Vehkamäki, H. From quantum chemical formation free energies to evaporation rates. *Atmos. Chem. Phys.* **2012**, *12*, 225–235.
- (120) Olenius, T.; Kupiainen-Määttä, O.; Ortega, I. K.; Kurtén, T.; Vehkamäki, H. Free energy barrier in the growth of sulfuric acid-ammonia and sulfuric acid-dimethylamine clusters. *J. Chem. Phys.* **2013**, *139*, 084312.
- (121) Wang, C.-Y.; Jiang, S.; Wang, Z.-Q.; Liu, Y.-R.; Wen, H.; Huang, T.; Han, Y.-J.; Huang, W. Can formaldehyde contribute to atmospheric new particle formation from sulfuric acid and water? *Atmos. Environ.* **2019**, *201*, 323–333.
- (122) Hanson, D. R.; Lovejoy, E. R. Measurement of the Thermodynamics of the Hydrated Dimer and Trimer of Sulfuric Acid. *J. Phys. Chem. A* **2006**, *110*, 9525–9528.
- (123) Kürten, A.; Münch, S.; Rondo, L.; Bianchi, F.; Duplissy, J.; Jokinen, T.; Junninen, H.; Sarnela, N.; Schobesberger, S.; Simon, M.; et al. Thermodynamics of the formation of sulfuric acid dimers in the binary ($\text{H}_2\text{SO}_4\text{-H}_2\text{O}$) and ternary ($\text{H}_2\text{SO}_4\text{-H}_2\text{O-NH}_3$) system. *Atmos. Chem. Phys.* **2015**, *15*, 10701–10721.
- (124) Dunne, E. M.; Gordon, H.; Kürten, A.; Almeida, J.; Duplissy, J.; Williamson, C.; Ortega, I. K.; Pringle, K. J.; Adamov, A.; Baltensperger, U.; et al. Global atmospheric particle formation from CERN CLOUD measurements. *Science* **2016**, *354*, 1119–1124.